Implications of Phase Change on the Aerodynamics of Centrifugal Compressors for Supercritical Carbon Dioxide Applications

Giacomo Persico
Laboratory of Fluid Machines (LFM)
Dipartimento di Energia, Politecnico di Milano
Via Lambruschini 4, 20156 Milano, Italy

Lorenzo Toni
Centrifugal Compressor and Expanders NPI
Baker Hughes, Nuovo Pignone
Via F. Matteucci 2, 50127 Firenze, Italy

Paolo Gaetani
Laboratory of Fluid Machines (LFM)
Dipartimento di Energia, Politecnico di Milano
Via Lambruschini 4, 20156 Milano, Italy

Ernani Fulvio Bellobuono
Centrifugal Compressor and Expanders NPI
Baker Hughes, Nuovo Pignone
Via F. Matteucci 2, 50127 Firenze, Italy

Alessandro Romei
Laboratory of Fluid Machines (LFM)
Dipartimento di Energia, Politecnico di Milano
Via Lambruschini 4, 20156 Milano, Italy

Roberto Valente
Centrifugal Compressor and Expanders NPI
Baker Hughes, Nuovo Pignone
Via F. Matteucci 2, 50127 Firenze, Italy

ABSTRACT

Closed Joule-Brayton cycles operating with carbon dioxide in supercritical conditions (sCO_2) are nowadays collecting a significant scientific interest, due to their high potential efficiency, the compactness of their components, and the flexibility that makes them suitable to exploit diverse energy sources. However, the technical implementation of sCO_2 power systems introduces new challenges related to the design and operation of the components. The compressor, in particular, operates in a thermodynamic condition close to the critical point, whereby the fluid exhibits significant non-ideal gas effects and is prone to phase change in the intake region of the machine. These new challenges require novel design concepts and strategies, as well as proper tools to achieve reliable predictions.

In the present study, we consider an exemplary sCO_2 power cycle with main compressor operating in proximity to the critical point, with an intake entropy level of the fluid lower than the critical value. In this condition, the phase change occurs as evaporation/flashing, thus resembling cavitation phenomena observed in liquid pumps, even though with specific issues associated to compressibility effects occurring in both the phases. The flow configuration is therefore highly non-conventional and demands the development of proper tools for fluid and flow modeling, which are instrumental for the compressor design. The paper discusses the modeling issues from the thermodynamic perspective and then highlighting the implications on the compressor aerodynamics. We propose tailored models to account for the effect of the phase change in 0D mean-line design tools as well as in fully 3D computational fluid-dynamic (CFD) simulations: the former was previously validated for sCO_2 compressors, the latter is validated in this paper against experiments of compressible flows of supercritical sCO_2 in nozzles. In this way, a strategy of investigation is build-up as a combination of mean-line tools, industrial design experience, and CFD for detailed flow analysis. The application of the design strategy reveals that the potential onset of the phase change might alter significantly the performance and operation of the compressor, both in design and in off-design conditions, according to three main mechanisms: incidence effect, front loading, and channel blockage.

Keywords: carbon dioxide; centrifugal compressor; phase change; barotropic model; supersonic flows; choking.

NOMENCLATURE

sCO_2	supercritical carbon dioxide
CFD	computational fluid dynamics
LUT	look-up table
P	pressure
T	temperature
ρ	density
c	speed of sound
h	specific enthalpy
I	specific rothalpy
s	specific entropy
v	absolute velocity
u	blade peripheral speed

x	nozzle axis
w	relative velocity
w_V	vapor mass fraction
Z	compressibility factor
M	Mach number
M_W	relative Mach number
$\dot{m}$	mass flow rate
η	polytropic efficiency
η_{TT}	total-to-total efficiency
β_{TT}	total-to-total pressure ratio
$(\cdot)_T$	total condition
$(\cdot)_C$	critical condition
$(\cdot)_1$	inlet condition
$(\cdot)_1^*$	impeller condition post leading edge
$(\cdot)_2$	impeller outlet condition
$(\cdot)_{SAT}$	saturation condition (at fixed entropy)

INTRODUCTION

The use of carbon dioxide in supercritical thermodynamic conditions (sCO_2) for closed Joule-Brayton cycles is attractive since it offers potential advantages in terms of cycle efficiency, size of the components, and dynamics of the system. As a result, sCO_2 power systems can efficiently convert energy from several sources, such as nuclear, concentrated solar, and waste-heat recovery, alternative to fossil fuels and, hence, instrumental for mitigating global warming from energy systems.

Depending on the specific heat source exploited, several layouts were historically proposed for sCO_2 power systems **[1]**. All of them, however, share the use of at least one compressor operating close the critical point, since the thermodynamic optimization of the cycle tries to minimize the compression work exchange driving the compression process towards high-density region. For cycle power capacities within 300 MW, the recommended machine is a centrifugal compressor **[2]**.

Besides large density and specific-heats gradients approaching the critical point [3], which couple with large departures from the ideal-gas behavior [4], phase-change phenomena can additionally occur because of local flow accelerations. Potential pitfalls associated

with two-phase operations, i.e. mechanical erosion, compressor performance and stability degradation to name a few, demand for a careful design of the main compressor to avoid premature shortcomings of the power cycles. To circumvent the two-phase problem, a safe margin from the saturation curve can be introduced depending on the expected Mach number [5], but the trade-off in terms of compression work might be not acceptable at higher Mach number ($M \geq 0.6$). An alternative margin can be formulated accounting for meta-stable equilibrium states [6], enabling single phase operation below the saturation dome. Nevertheless, the experimental results are limited to the right branch of the saturation dome ($s/s_c \geq 1$), while no evidences are presently available for the left-branch ($s/s_c \leq 1$) of interest to sCO_2 power systems. On top of that, the reduction of the transition limit is still not sufficient to exclude phase change at all, especially close to the critical point.

Opposed to these negative expectations, Noall & Pasch [7] reported stable and efficient operations for a full-scale compressor, including intake-flow conditions within the saturation dome. The smaller liquid-to-vapor density ratio, e.g. compared to cavitating pump, was recognized as responsible for the lack of detrimental effects. Nonetheless, there were neither flow-field measurements nor clear physical explanations to support this conjecture. In this context, computational fluid-dynamic (CFD) simulations can provide a deeper insight into the potential impact of multi-phase flows on the compressor aerodynamics.

Previous attempts [8, 9, 10, 11] at simulating two-phase sCO_2 flows were successfully performed on the Sandia main compressor [12]. Although the available experimental data enable the validation of the computational model, the Sandia benchmark is a sub-scale prototype delivering a relatively small pressure rise. The corresponding low velocities ($M \leq 0.4$ [9]) explain the limited phase-change fraction seemingly affecting Sandia's compressor operations. Full-scale high-loaded compressors are expected to suffer more from phase-change phenomena, pointing to the need for reliable tools to predict them and for a better understanding of the flow physic and its implication on compressor performance and rangeability.

After some thermodynamic considerations about suction-induced phase-change phenomena, we detail the computational strategy, consisting in both mean-line and CFD calculations. Main computational difficulties in simulating two-phase flow close to the critical point are highlighted; then, we apply our computational methodology to analyze the flow field of an exemplary full-scale compressor. The analysis elucidates the phase-change implications on compressor aerodynamics, both in design and off-design conditions.

THERMODYNAMIC FRAMEWORK

The optimization of sCO_2 thermodynamic cycles drives the compressor intake condition towards the critical point, paving the way for potential two-phase flows during machine operation.

Figure 1 depicts the thermodynamic framework at the intake of a sCO_2 compressor, constructed by resorting to the Span-Wagner

thermodynamic model of the fluid **[13]** as implemented in REFPROP **[14]**. Considering supercritical cycles, the thermodynamic optimization suggests setting the intake compressor condition in the white area highlighted in the figure. As visible from the contours of compressibility factor Z depicted in the one-phase region, the intake features severe real-gas effects, in terms of volumetric departure from the ideal-gas model, and lower entropy level with respect to the critical value **[5]**. Moreover, the optimization is usually constrained by the minimum available temperature of the cycle: the lower the temperature, the higher the cycle efficiency.

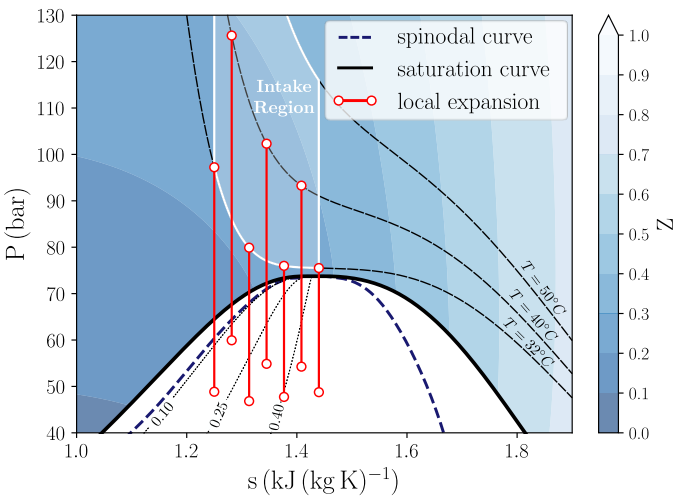

FIGURE 1: ENTROPY-PRESSURE STATE DIAGRAM OF THE CO_2, INCLUDING THE SATURATION AND THE SPINODAL LINES, WITH INTAKE ISENTROPIC SUCTIONS.

In such context, the intake conditions are always close to saturation. Assuming isothermal lines at 32° C and 40°C, corresponding to low-temperature and relatively high-temperature heat sinks, seven exemplary compressor intake conditions are considered in Figure 1. As well known, the intake of a turbo-compressor features nearly-isentropic suction phenomena, induced by the flow-turning around the leading edge of the blades and by the acceleration due to the blade blockage. These local expansions might even exceed 30% of the enthalpy rise of the compressor. The combined thermodynamic and aerodynamic optimization proposed by Romei et al. **[15]** indicates that a pressure ratio of approximately 3 is optimal for sCO_2 power systems.

Applying such findings in the present context, and considering isentropic expansions, the red lines in Figure 1 highlight the suctions that might occur in local regions of the compressor intake. All of them penetrate significantly within the two-phase region; moreover, since the entropy level of such expansions is smaller than that of the critical point, the phase-change occurs as cavitation/flashing, with vapor quality ranging from 0.1 to almost 0.5 in the point of minimum pressure. For completeness, Figure 1 reports the spinodal lines (dashed lines) alongside the saturation ones, to highlight the extension of the region of potential meta-stable states. As clearly visible, the spinodal line for entropy lower than the critical one is much closer to the saturation line than the other, and all the suction lines reported exceed the spinodal limit. This indicates that, in the present class of compressors, the phase change does occur, even if in some local regions one may observe meta-stable states. For this reason, the phase change or at least its effects on the flow within sCO_2 compressors have to be introduced in any design or simulation tool. In the next section we discuss the computational issues prompted by the real-gas effects and by the phase change, as well as the approach devised to introduce such effects within engineering-relevant computational models.

AERODYAMIC MODELING OF sCO_2 COMPRESSORS

The aerodynamic design and analysis of centrifugal compressors is usually carried out with multiple models, featuring different levels of fidelity and computational cost. In the present work, a zero-dimensional model, based on mean-line balances between the inlet and the outlet of each component, and an aerodynamic fully-3D model are used in the investigation of a sCO_2 centrifugal compressors operating in close proximity of the critical point. Both the mean-line and the CFD models require proper treatments for the thermodynamic modeling of the fluid, considering both the real-gas effects of the fluid in the single-phase condition and the effects of the phase change in the two-phase region. However, the CFD model demands a specific and non-conventional formulation due to the distributed flow representation, which requires the explicit resolution of multi-phase regions of the flow. To pursue this objective in a computationally robust and efficient way, we propose a novel formulation whose mathematical concept, thermodynamic foundation, and experimental assessment are discussed in this Section. The mean-line tool will be discussed in the following section alongside its application to the prototype compressor studied in this work.

1 CFD model for aerodynamic simulation of sCO2 compressors

The CFD model applied in this study was conceived as a result of the experience gained by the LFM group of the Politecnico di Milano in a decade of simulations on high-speed turbomachinery, including machines operating with fluid in highly non-ideal conditions. The model is based on the ANSYS-CFX finite-volume flow solver, selecting the high-order total variation diminishing (TVD) numerical scheme for the inviscid fluxes and the central difference scheme for viscous terms as implemented in the code. The effects of turbulence are introduced via the k-ω SST model proposed by Menter [16], assuming fully turbulent flow. Automatic application of wall function is specified, so that the code switches from near-wall resolution to the application of wall functions on the basis of the local value of the y^+.

The equations of motion are solved on structured meshes composed by hexahedral elements. Meshes are generated applying AutoGrid™ and include the intake duct, the impeller, with fillet radii, and the diffuser. Only closed impellers and vaneless diffusers are considered. Since the study is oriented to the study of the aero-thermodynamics of the flow within the blades, with a specific focus on the intake region of the impeller, the secondary flow within the seals and the corresponding leakage flow are not modelled (see, for example, [17] for the impact of such effects on the simulation of centrifugal impellers).

The successful application of this CFD model to sCO_2 compressors demands a highly non-conventional thermodynamic treatment to face the issues highlighted in the previous section. Even neglecting any excursion within the two-phase region, severe real-gas effects arise throughout the compression of the flow across the machine. Considering the exemplary intake conditions marked in Figure 1, and

a pressure ratio of 3 across the compressor, the compressibility factor Z rises from 0.1-0.2 at the intake to 0.4-0.5 at the diffuser exit. To this end, a LUT is built using the intensive quantities (P, T) as primitive variables, complying with the implementation of real-gas properties in ANSYS-CFX.

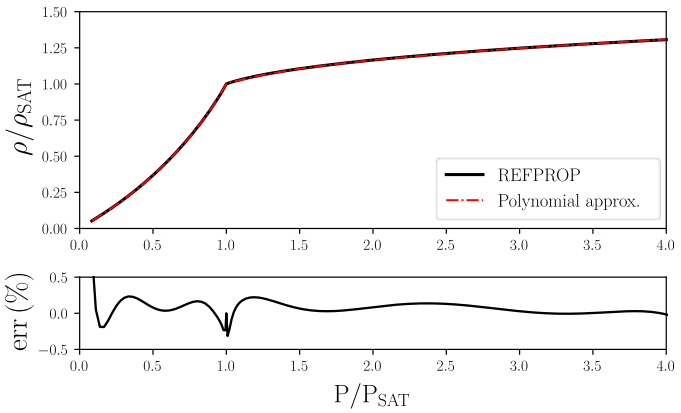

FIGURE 2: PRESSURE-DENSITY RELATION ALONG AN ISENTROPIC TRANSFORMATION, INCLUDING THE TWO-PHASE AND THE SINGLE-PHASE REGIONS

In this study, a first CFD model was constructed by resorting to the standard LUT approach recalled above; however, such model proved to be unsuccessful for any of the simulations of interest. As pointed out in the previous section, in the present thermodynamic context the phase change does occur and, hence, a thermodynamic model using only intensive quantities as primitive variables fails in representing the two-phase states. Even though the LUT was extended up to the spinodal limit, as shown in Figure 1 the local expansion on the blades drives the fluid condition beyond the spinodal limit, in the region where two phases necessarily co-exist. In this context, two alternatives are possible: (i) simulating the non-equilibrium process that leads to generate a heterogeneous mixture of liquid and vapour from the supercritical fluid; (ii) modeling the mean effects of phase change, considering a homogenous fluid with mean specific properties, evaluated as a weighted averages of the properties of the two phases.

The 'simulation' approach is, in principle, the most accurate between the two ones and could be theoretically able to predict the actual physical process with high fidelity; however, it requires a time-dependent approach similar to the ones implemented for the study of cavitation in the liquid pumps. The complexity of the model, which is still in the development phase (see [11] for a first application to sCO_2 systems) and the computational cost involved make this approach still not suited for routine engineering application.

The 'model' approach is, instead, more attractive for engineering interests, as it allows simulating the flow within the compressor in presence of phase change without solving the actual unsteady phase-change process but representing only its time-mean effects. Especially, it allows to highlight, at reasonable computation cost, the zones of the compressor that might be exposed to cavitation, thus providing a fundamental tool for evaluating the quality of the compressor design.

For these reasons, in this study the 'model' approach was selected and the detail of its implementation in the sCO_2 context are discussed in the following. The phase change can be introduced in a simplified way also in the context of homogeneous equilibrium models, by adding proper source terms in the flow equations. Such approach was proven to predict in a reasonable way the effects of phase-change in sCO_2 nozzles and compressors [10] but it requires to calibrate a few empirical parameters and to put special care in the

definition of the computational mesh. With the aim of constructing a flow model as simple and robust as possible, and thus suitable for routine industrial application, we propose an alternative approach.

As well known, the fluid exhibits a significantly different volumetric behaviour inside and outside the two-phase region. In general, the specific volume of the fluid is a function of pressure and temperature. However, if the thermodynamic transformation is known, the formulation can be simplified into a univocal dependence of the density on pressure, which 'embeds' the associated temperature rise. This latter formulation, called barotropic relation in the scientific literature, has the advantage of removing explicitly thermal effects from the mass and momentum balance equations, thus decoupling the mechanical equations from the thermal one.

Figure 2 provides an example of the barotropic relation $\rho = \rho(P)$ evaluated along an isentropic transformation for a value of s/s_C included in the range 0.9—1. The plot extends the law from very low pressure in the two-phase region ($P/P_{SAT} = 0.1$, x= 0.5) up to the supercritical fluid region ($P/P_{SAT} = 4$), crossing the saturation condition, sampled from the Span-Wagner model implemented in REFPROP. The line indicates two very different compressibility between the two-phase and the singe-phase zones, suggesting that an abrupt change in the speed of sound occurs between the two conditions. The speed of sound in a two-phase mixture is not univocally defined, depending on whether mechanical and thermal equilibrium can be assumed between the two phases. In the limit of infinitely homogenized vapour bubbles in a liquid free-stream, the heat and mass transfer between phases occur at a higher rate than the propagation of the sound wave, and hence thermal equilibrium can be assumed [18]. Assuming also no relative motion between phases, the speed of sound within the saturation dome can be casted as:

$$c = \sqrt{\left(\frac{\partial P}{\partial \rho}\right)_s} \tag{1}$$

where ρ is the density of the two-phase mixture, defined on the basis of the vapour quality.

As a result of these assumptions, the speed of sound exhibits an abrupt drop across the saturation line. The aerodynamic implication of this behaviour, its physical validity, and its technical relevance in practical engineering applications will be discussed later.

On the modeling ground, polynomial functions provide very accurate approximations of the two distinct branches of the barotropic law (five-order polynomials are used in this work). To combine the two polynomial expressions in a single analytical model we resort to a logistic function defined as follows:

$$f(P) = \frac{P - P_{SAT}}{\sqrt{1 + (P - P_{SAT})^2}} + 1 \tag{2}$$

The selection of the thermodynamic transformation along which the P-ρ expression is interpolated needs discussion. In first approximation, the isentropic compression can be considered; as an alternative, the entropy increase estimated by the mean-line calculation can be used to model the volumetric behaviour of the fluid across the compression; in this way, the re-heat effect of the losses is taken into account.

Before focusing on the actual compressor configuration, we discuss in the next section the assessment of the barotropic modeling by comparing CFD predictions with experiments performed on a converging-diverging nozzle available in scientific literature.

2 Assessment of barotropic modeling for the numerical simulation of high-speed flows of sCO_2

The experiments performed by Nakagawa et al. [19] were considered to assess the capability of the barotropic model in representing the physics of sCO_2 high-speed flows, which might involve the specific phase transition of interest for the present sCO_2 application (liquid ↦ vapour). Temperature (from thermocouples) and pressure (from strain gauges) measurements were measured along the axis of a converging-diverging nozzle and were documented for several operating conditions and nozzle geometries. In the present work, the expansion process closer to the thermodynamic critical point ($T_{T0} = 37.3\ °C, P_{T0} = 91\ bar$ corresponding to $s_0/s_c = 0.95$) was selected to illustrate the potential of a barotropic modeling for simulating sCO_2 flows.

For the present validation, the CFD model is implemented in ANSYS-Fluent 19.1, so that a two-dimensional computational domain is employed, whose mesh is reported in Figure 3 (top). Among the configurations tested by Nakagawa and co-authors, the nozzle having a divergence angle of 0.153° was considered, producing an outlet pressure of 27.5 bar when expanding from the above intake conditions. The corresponding isentropic expansion is depicted in Figure 3 (left). It is worth to underline that, for the conditions of interest, the meta-stable region is limited, and it is expected not to have an appreciable role in the phase transition. Moreover, the expansion falls perfectly within the thermodynamic region of interest for the present class of sCO_2 compressors, highlighted in Figure 1.

Adiabatic and no-slip boundary conditions are applied to the wall, while a symmetry condition is imposed on the nozzle axis. The two-equation k-ω SST model [16] is used to account for the effects of turbulence, specifying a hydraulic diameter of 10 mm and the eddy-viscosity-ratio of 2.5 at the inlet section. With respect to the small scale of the experiments, the wall roughness proved to be non-negligible; following [20], an average roughness of 2 μm was estimated for the nozzle walls, resulting into an equivalent sand-grain roughness $k_s = 6.2\ \mu m$. Wall functions accounting for the surface roughness were selected, since the presence of surface roughness dictates a first-layer distance greater than the roughness itself, resulting at the throat in a centre-cell distance from the wall of $6.7 \times 10^{-6}\ m$. In the present mesh, this discretization was obtained with 9 uniformly spaced layers disposed along the y-direction. The grid resolution at the throat is $2 \times 10^{-5}\ m$ along the x-direction. A dedicated grid-convergence study halving and doubling the number

of elements along the x-direction showed no quantifiable variations in the distributions of main thermodynamic and fluid-dynamic quantities along the nozzle axis. All governing equations were discretised with a third-order QUICK scheme. The PRESTO! Scheme is used to interpolate the pressure at the cell face, while the gradient is reconstructed with a Green-Gauss node-based technique.

The comparison between simulation and experiment is reported in Figure 3 (right) in terms of pressure distribution along the nozzle axis, in which the temperature measurements are converted into pressure values assuming thermodynamic stable equilibrium (meta-stable states are neglected). The experimental-numerical agreement is remarkable, showing that the barotropic model can be a robust and cost-effective solution to simulate such a high-complex flow. Moreover, significant flow quantities that are not explicitly computed by the model can be retrieved as a post-process. Specifically, under the assumption of constant total enthalpy (or rothalpy I in a rotating frame), the static enthalpy can be estimated from the velocity field, i.e. $h = h_T - 0.5v^2$ ($h = I + 0.5u^2 - 0.5w^2$ in a rotating frame). Then, such information can be used along with the pressure to obtain any desired properties under the thermodynamic equilibrium assumption. Following this procedure, the vapour fraction was computed and it is reported in Figure 3 (right). It has to be noted that such vapour fraction distribution is fully consistent with the results of the homogeneous equilibrium model (HEM) that explicitly accounts for thermal effects and the actual entropy level. The interested reader can find additional validations of the present methodology against different operating conditions, computational strategies and phase-change phenomena in [21].

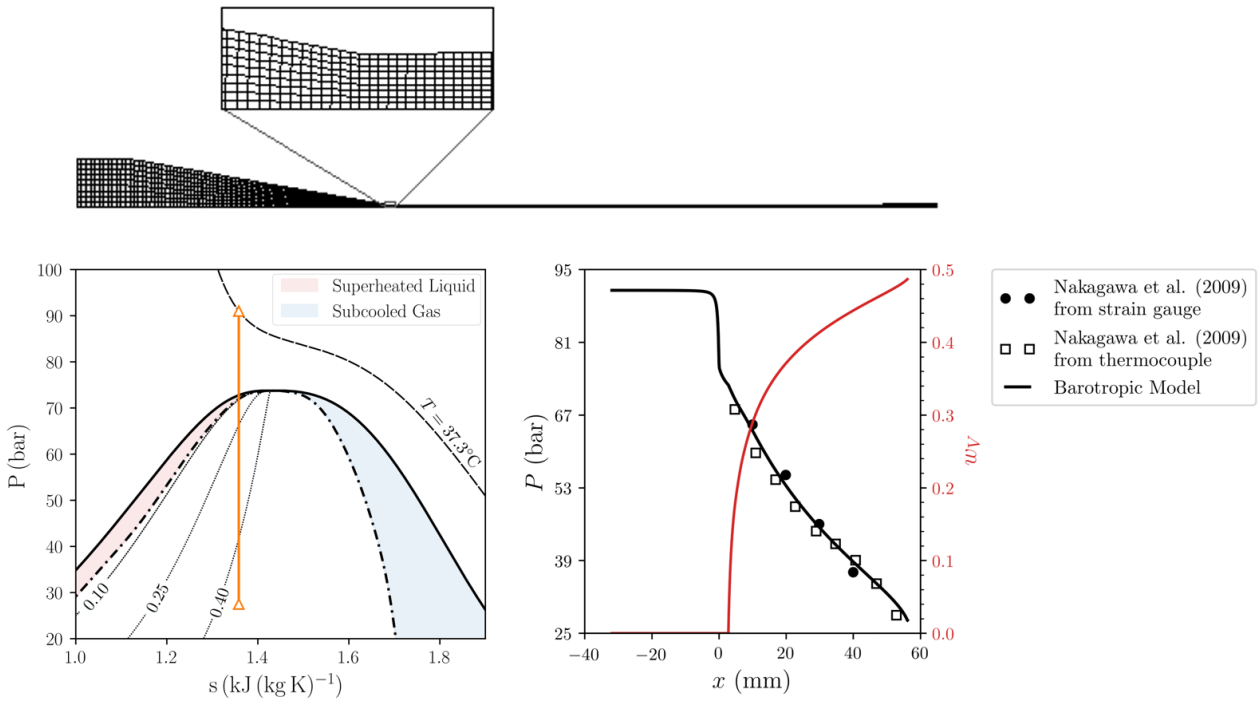

FIGURE 3: EXPERIMENTAL-NUMERICAL COMPARISON OF SCO_2 HIGH-SPEED FLOW IN A NOZZLE. TOP: COMPUTATIONAL DOMAIN AND MESH. BOTTOM: STATE DIAGRAM WITH THE ISENTROPIC EXPANSION (LEFT); PRESSURE AND VAPOUR MASS FRACTION ALONG THE NOZZLE AXIS (RIGHT).

PROTOTYPE sCO_2 COMPRESSOR CONFIGURATION AND OVERALL MEAN-LINE ANALYSIS

Among the several conditions investigated, we focus on a compressor intake condition given by $P_{T1}/P_C = 1.09$ and $0.9 < s_1/s_C < 1$, for illustrative purposes. For the given application, the impeller flow coefficient and the peripheral Mach number fall within the common envelope of Oil & Gas applications; therefore, a typical centrifugal impeller geometry, belonging to Baker Hughes database of stages, has been considered for the present investigation. Since this work is focused on the basic effects of phase change on the aerodynamics of the impeller blades, only the intake duct, the impeller and the diffuser are considered in the computational models. The IGV and the leakage cavities are excluded from the analysis, since they are deemed not crucial for the physical mechanisms investigated. No swirl is given to the flow entering the impeller.

The impeller has a mainly radial meridional architecture, with limited extension of the inducer. The impeller features backward blading to reduce the absolute velocity and guarantee an efficient diffusion process. The rotor is shrouded and the sealing, located at the impeller eye, reduces the recirculating mass flow to less than 2%. The diffuser is vaneless, to allow the highest possible rangeability.

Prior to focus on the detailed compressor aerodynamics, the overall performance and operation of the machine are analysed on the basis of a mean-line representation. The mean-line analysis, performed with the in-house tool of Politecnico di Milano, allows for the comprehension of the macro-phenomena occurring in the machine (notwithstanding the impossibility of calculating the local flow field). Section by section, the mean parameters are calculated under the approximation of pitch-wise average at the inlet section and pitch-/span-wise average at the outlet one: at the rotor inlet, relative velocities consider the radial blade evolution. In the following of this section we first recall the mean-line tool and its features tailored for sCO_2 applications, and then discuss the mean-line performance of the prototype compressor.

1 Mean-line tool for sCO_2 compressors

The code was conceived for both the design of new machines and the verification of existing ones. In the present study existing geometries were calculated. The code was validated and tuned using the experimental data available at the Laboratory of Fluid-Machines [22] and in the open literature. Of particular interest for the present context, a successful validation was performed for the Sandia-Lab sCO_2 compressor, resulting in estimates of the compressor total-total efficiency within ±1.5% of the experimental value.

The code implements several loss correlations for all the typical components of centrifugal compressors; the loss models include several terms depending on the component under consideration. For the present research, the models can be divided in two groups:

- IMPELLER: incidence [23], friction [24], recirculation [24], diffusion [25] and mixing [26] losses; the slip factor estimate is included as well, using the Stanitz correlation corrected for the splitter blade [27].

- VANELESS DIFFUSER: friction losses on the endwalls, with a check on the diffuser stability [28]. A pinch can be also introduced at any radial coordinate and of any extent.

This set of losses includes the main entropy-generation mechanisms also accounted in the following CFD calculations, enabling a fair comparison between the mean-line and CFD predictions.

In each relevant section of the machine, the balance equations are solved by resorting to the Span-Wagner thermodynamic model. Since the calculation has to treat two-phase conditions, multiple alternatives are possible for setting the point of phase transition. Following a conservative choice about the onset of phase change, the thermodynamic model was constructed by setting the phase change at the saturation [5], neglecting the potential delay introduced by meta-stable phenomena. This thermodynamic set-up was applied to the prototype compressor, whose overall operation and performance features are discussed in the next subsection.

2 Mean-line performance and operation of the prototype sCO_2 compressor

Figure 4 summarizes the main results of the application of the mean-line code to the prototype compressor. In particular, Figure 4(a) provides the trends of total pressure ratio, diffusion factor and total-total efficiency, made non-dimensional with respect to the relative design values for confidentiality reasons. The trends indicate that the present machine shows an efficient behaviour on the whole range. It is to be noted that fully turbulent flow conditions can be assumed for all the points of the curve, thanks to the very low kinematic viscosity of the sCO_2.

In terms of rangeability, the low flow rate limit is here conventionally defined as the condition at which the diffusion factor $W_2/W_{1t} = 0.6$; the definition of the upper limit is, instead, much more critical in case of sCO_2 compressors. In conventional gas compressors, the performance curves exhibit an inherent limitation at high flow rate due to the onset of a sonic throat within the impeller or the diffuser. The mean-line model does not show such a feature in none of the characteristic curves, up to 150% of the design flow rate. However, a thermodynamic analysis of the mean-line solution reveals that the intake region of the impeller is prone to phase change. The onset of phase change is of relevant concern for the designer, for both the change in the volumetric behaviour of the fluid and the abrupt reduction of speed of sound as the fluid becomes a mixture of liquid and vapour, which ultimately might alter the choked-flow condition.

To clarify the issue, a specific procedure was implemented in the mean-line code to analyse the intake region. At first, the thermodynamic process from the inlet compressor flange to the impeller inlet can be proficiently approximated as an isentropic expansion. This consideration allows for an easy application of the energy balance and of the continuity to get the blade-inlet static condition. Once the flow approaches the blades, their blockage induces a further acceleration and, especially, a further suction, thus exposing the whole channel to the risk of phase change. Even though it does not provide the detailed flow, the mean-line approximation

allows at least to evaluate the expansion due to the blockage at the leading edge. Figure 4b reports the trend of static conditions in terms of pressure by varying the flow rate. The proper design of the rotor inlet section (i.e. the blade number and thickness, the hub/tip diameters) may reduce the flow velocity, having in mind that the condition $V_1 < \sqrt{2(h_{T1} - h_{SAT})}$ must hold to remain above saturation in the intake duct. In particular, the blade thickness plays a growing role as the flow rate increases, as visible by the different trends in the static pressure, upstream (P_1) and downstream (P_1^*) of the leading edge. Figure 4(b) also reports the relative Mach number at the blade midspan section (as representative of the whole channel) downstream of the blade leading edge. Even though highly simplified (as it will be clear from the distributed flow analysis reported in the next Section), the combination of moderate flow velocity and the very low speed of sound in the two-phase zone may lead to supersonic flows at 130% of the design flow rate.

Eventually, for the present compressor the mean-line analysis predicts a flow-rate range between 80% and 130% of the design value.

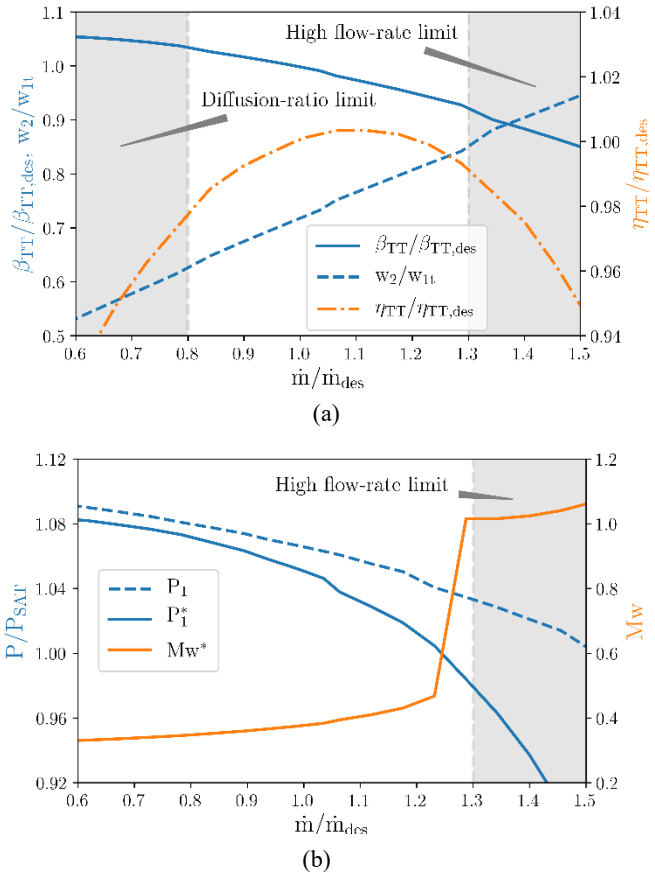

FIGURE 4: MEAN-LINE PREDICTION. (a): COMPRESSOR PERFORMANCE CURVES; (b): DEPENDENCE OF THE SUCTION ON THE FLOW RATE

sCO_2 COMPRESSOR AERODYNAMICS

In order to achieve a realistic picture of the flow within the compressor under study, fully 3D CFD simulations were performed by resorting to the barotropic model of the sCO_2. Prior to its routine application within CFD calculations, the model has to be calibrated on the actual thermodynamic condition at which the compressor operates. The barotropic relation $\rho = \rho(P)$, indeed, depends on the entropy level of the fluid at the intake and on the thermodynamic path of the transformation. If one assumes an isentropic transformation, the barotropic relation is univocally defined from the compressor intake condition. It is to be noted, however, that such an assumption for the barotropic model does not imply that the compression process of the fluid within the machine is isentropic, but only that the inevitable entropy rise across the machine does not affect the density of the fluid.

In order to assess the validity of the isentropic barotropic model for sCO2, comparative CFD simulations were performed with both

the barotropic model and the standard LUT approach, based on the Span-Wagner model. Then, the compressor in realistic operating conditions, closer to the saturation dome, are considered.

1 Construction of the barotropic model for sCO_2 compressors

Comparative barotropic and LUT simulations were performed by Politecnico di Milano considering at the intake $P_{T1}/P_C = 1.63$, $T_{T1}/T_C = 1.045$, which are sufficiently far from the saturation, thus avoiding phase change within the machine. The LUT was constructed using the REFPROP library and following the guidelines provided in [3], i.e. with resolution equal to 0.1 K in temperature and 0.25 bar in pressure. Trials with higher resolution did not show any variation in the solution.

The simulations were performed onto multiple computational meshes composed by hexahedral elements, with progressively increasing resolution to achieve a grid independent solution. Eventually a grid composed by 4 million of cells was selected, featuring maximum y^+ on the blade walls of 2-3 and y^+=50-100 at the endwalls.

Simulations were performed assigning at the inlet the total pressure, purely meridional flow, turbulence intensity equal to 5% and eddy viscosity ratio equal to 1; at the outlet, the flow rate was assigned. The LUT-model also requires assigning the total temperature at the inlet, evaluated consistently with the total pressure and entropy levels at the intake. On the other hand, simulations performed with the barotropic model do not require the temperature specification, as the energy equation is not solved. The flow rate value was chosen so to guarantee that the volumetric flow rate is equal to the one in the design thermodynamic conditions (thus scaling the effect of density change between the two conditions).

The simulations showed a smoother and faster convergence process in case of barotropic model with respect to the LUT one, also thanks to the lower number of equations to be solved for the former; the final residuals resulted of the same order of magnitude. The comparison between the two models allows quantifying the different impact of the local entropy production on the density field, which is neglected by the barotropic model. Figure 5, which compares the distributions of density on the midspan blade-to-blade surface for the two simulations, clearly shows that the such differences are really minor and do not alter the flow configuration. In more quantitative terms, the maximum differences in density are of the order of 0.1% in the free-stream region and rise to 0.5% in local regions of the boundary layer / dead water zones where the peak entropy are found.

The differences in terms of total and static pressure were found to be comparable with the density estimates, i.e. $\pm$0.2%. The difference in overall total pressure ratio, and hence in the polytropic efficiency, results about 0.05%.

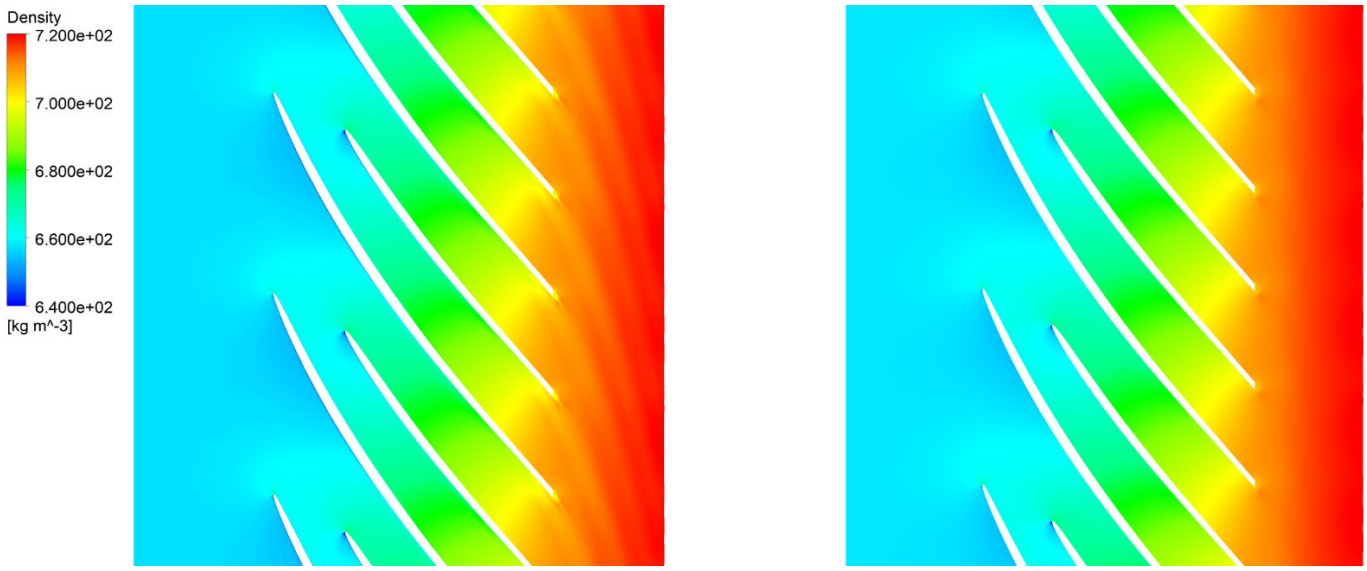

FIGURE 5: DENSITY FIELDS ON THE BLADE-TO-BLADE SURFACE AT MIDSPAN EVALUATED FOR THE LUT (LEFT) AND BAROTROPIC (RIGHT) MODELS IN PURE SINGLE-PHASE SIMULATION

A further relevant quantity of interest is the speed of sound, which is more difficult to reproduce, because of its inherent differential definition; however, it is extremely relevant in the context of compressible flow and even more in case of phase change. Figure 6 compares the distribution of speed of sound for LUT and barotropic simulations. Again, the barotropic model is able to capture the distribution; the maximum quantitative differences are slightly higher than those for the other quantities, namely of the order 1 %, which is comparable with the inherent uncertainty of the thermodynamic model [13].

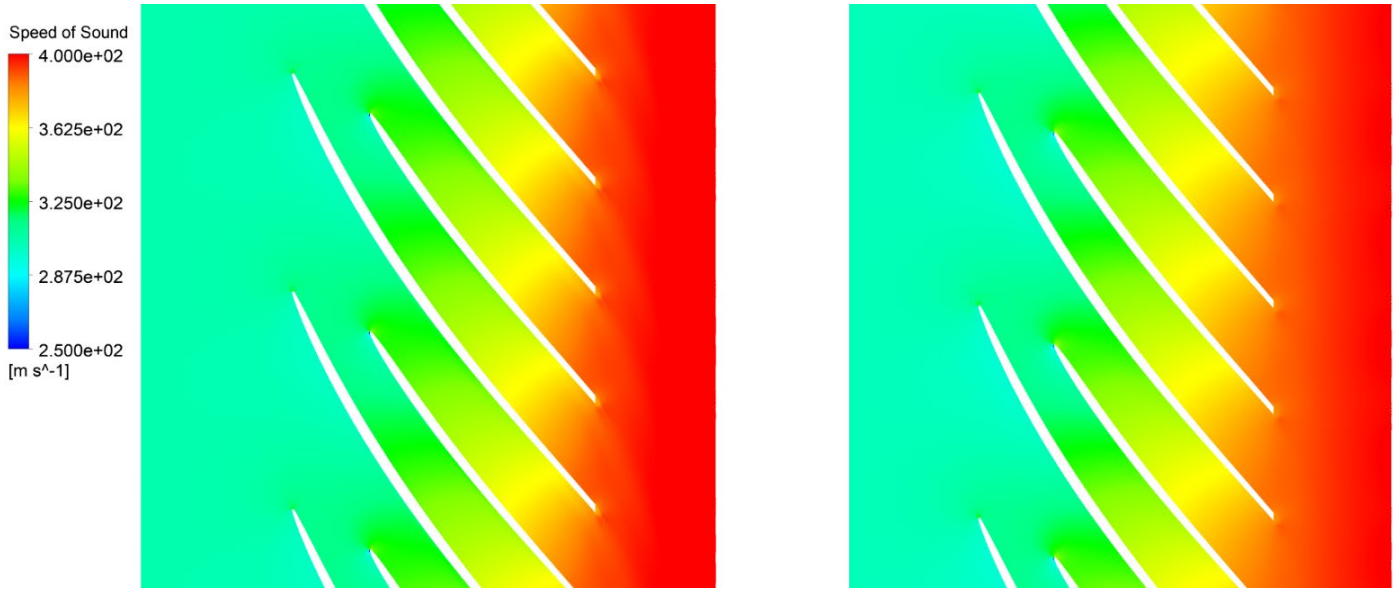

FIGURE 6: DISTRIBUTIONS OF SPEED OF SOUND ON THE BLADE-TO-BLADE SURFACE AT MIDSPAN EVALUATED FOR THE LUT (LEFT) AND BAROTROPIC (RIGHT) MODELS IN PURE SINGLE-PHASE SIMULATION

These results indicate that the barotropic model constructed assuming isentropic law is able to predict the flow of sCO_2 within a centrifugal compressor with a high level of accuracy, at least in the single-phase zone where comparative LUT simulations are feasible.

2 sCO_2 compressor aerodynamics with phase change

The selected intake conditions of interest are considerably closer to the saturation than the one considered in the previous analysis. Two more realistic thermodynamic states are now simulated, by applying the barotropic model of the sCO_2 to conditions featuring at the intake reduced total pressure equal to $P_{T1}/P_C = 1.36$ and $P_{T1}/P_C = 1.09$ respectively, with the same entropy level belonging to the range 0.9—1; the two conditions are representative of respectively high (~40°C) and low (~33°C) temperature heat sinks.

First considering the high-temperature condition, no macro-traces of the phase change appear in the distributions of density and speed of sound, as shown by the plots in Figure 7, which reports the same quantities on the blade-to-blade surface at 10% span; however, close to the leading edge of the main blade and, especially, of the splitter blade, very local drops of pressure take place, penetrating within the dome at a sufficient extent to make critical the LUT simulations (that indeed did not converge in this case). This technical difficulty highlights a physical phenomenon that one can properly appreciate only by resorting to CFD. In the mean-line analysis of the sCO_2 compressor, an attempt was made to estimate the choking limit by considering the impact of phase change; in that context, however, only mean-line estimates are available and the phase change is predicted to occur only at very high flow rate. The CFD simulation shows that the local shape of the blade in the leading area, along with a non-zero incidence, are crucial for the onset of phase change, which may occur already in design condition.

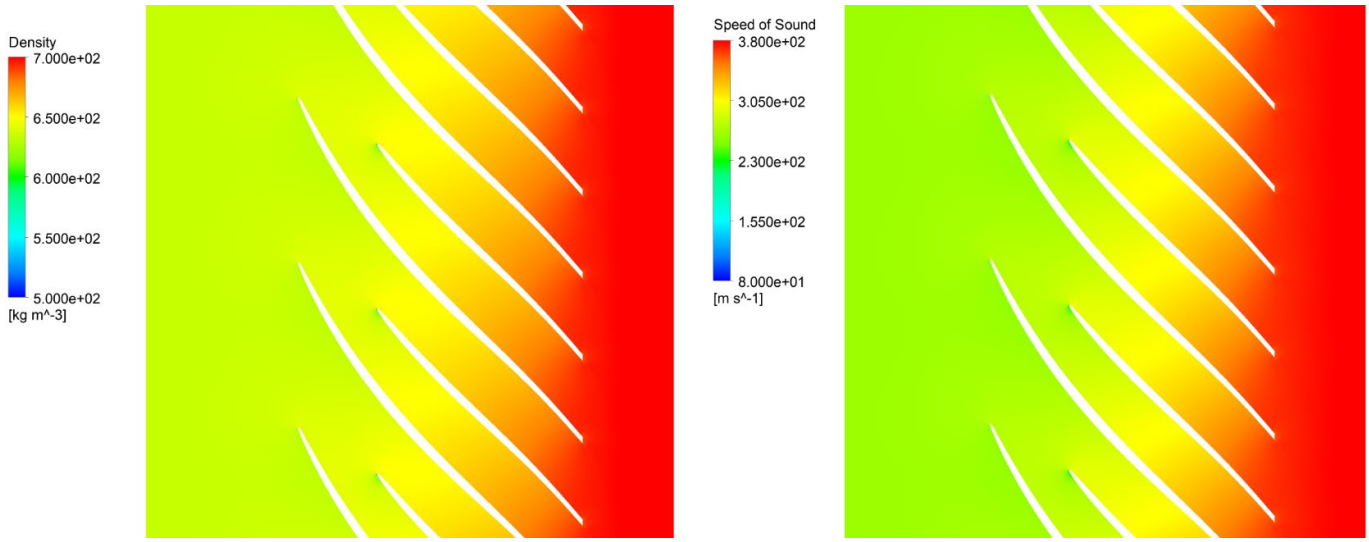

FIGURE 7: DISTRIBUTIONS OF DENSITY (LEFT) AND SPEED OF SOUND (RIGHT) ON THE BLADE-TO-BLADE SURFACE AT 10% SPAN FOR HIGH-TEMPERATURE INTAKE CONDITION

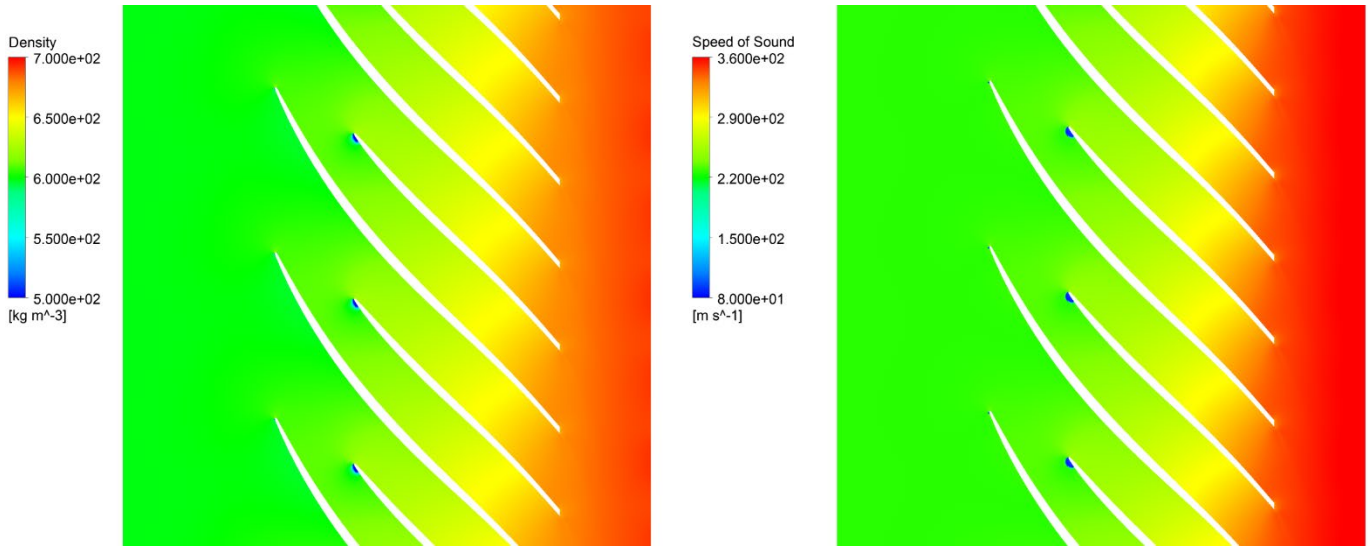

FIGURE 8: DISTRIBUTIONS OF DENSITY (LEFT) AND SPEED OF SOUND (RIGHT) ON THE BLADE-TO-BLADE SURFACE AT 10% SPAN FOR LOW-TEMPERATURE INTAKE CONDITION

As a proof of that, simulations at low temperature (which is the actual design condition for this compressor) exhibits the onset of phase change on wide areas of the compressor intake. Figure 8 shows the same quantities on the same surface (and with the same scales) of Figure 7. Both the density and the speed of sound drop significantly in proximity of the leading edge of the main blade and, especially, of the splitter blade. As well known, the turn of the flow around the leading edge of a blade is associated to an expansion, which is normally larger on the suction side of the leading edge. This is very localized if the incidence angle of the flow with respect to the blade is nearly null, as it occurs for the main blade. The splitter blade, on which the control of the incidence angle is more difficult due to the azimuthal gradients within the channel, operates instead with positive incidence, and the suction region is much wider. The drop of speed of sound, in particular, marks the region where phase change occurs, according to the model. By processing the flow field with thermodynamic models, the vapour quality reaches 0.25 in the front part of the splitter blade. The character of the flow does not change at midspan.

The impact of such effects on the compressor aerodynamics appears to be minimal, even though the implication on the mechanical integrity of the blades should be verified, also considering that the leading-edge zone is the thinner part of the blade. The impact of the phase change on the aerodynamics of the compressor becomes much more relevant in the shroud region of the compressor. Figure 9 reports the distribution of density, speed of sound and relative Mach number at 90% span. In this case, the incidence is nearly null for both the main blade (on which it is even slightly negative) and the splitter blade. However, the simulation indicates the onset of a wide region of phase change on the suction side of the blade, not directly connected to the flow turning around the leading edge; at the same time, the suction occurs upstream of the bladed channel, where the suction due to blade blockage occurs. For velocity triangle

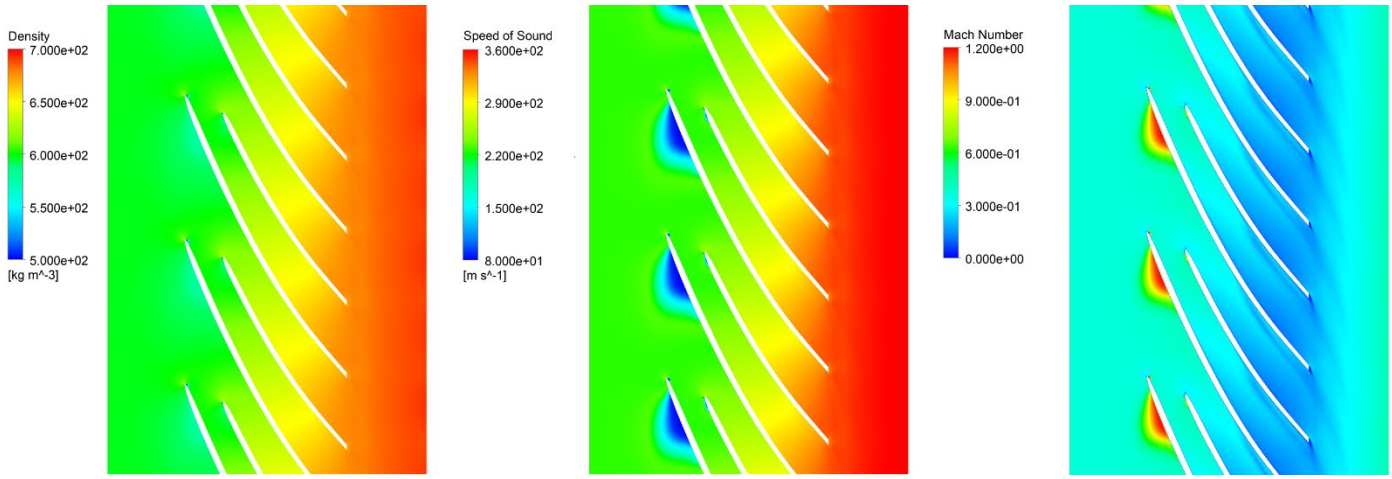

FIGURE 9: DISTRIBUTIONS OF DENSITY (LEFT), SPEED OF SOUND (CENTRE), AND RELATIVE MACH NUMBER (RIGHT) ON THE BLADE-TO-BLADE SURFACE AT 90% SPAN FOR LOW-TEMPERATURE INTAKE CONDITION

composition, the tip region features the highest relative Mach number. Moreover, the front loading activated by the flow turning in the front part of the blade induces suction that triggers the phase changes. This latter, in turn, prompts a sudden drop in speed of sound, translating into a sudden rise of relative Mach number, which drives the flow regime to transonic in an otherwise nearly incompressible operation of the machine. In the core of the two-phase region, the density and pressure are consistent with a vapour quality of 0.05. It is not known if such two-phase effects occur in the actual operation of the compressor, since deviations from either the thermal or the mechanical equilibrium assumption might take place. However, since the tip region of the blade is the most critical for the mechanical integrity, and the region of potential two-phase onset is relatively wide, the present results indicate that the topic should be carefully considered in future experimental studies.

In the present condition, we are probably at the margin at which two-phase effects become relevant: whenever $P_{T1}/P_C < 1.09$ and $0.9 < s_1/s_C < 1$ or, at the same reduced thermodynamic states, the compressor operates at off-design conditions, the impact of phase change on the compressor aerodynamics is expected to be prominent. The next section discusses in detail this latter issue.

IMPACT OF THE PHASE CHANGE AT OFF-DESIGN OPERATION OF sCO_2 COMPRESSOR

As pointed out in the mean-line analysis, the off-design operation of the present centrifugal compressor can lead to transonic flow regime at high flow rate (130% of the design one), based on consideration about the blade blockage. The CFD analysis indicates that such transonic effects can occur locally even in design operation. For this reason, we now focus on an intermediate off-design condition, namely for flow rate equal to 110% of the design value.

Figure 10 reports the corresponding distributions of density, speed of sound and relative Mach number at midspan. The two phase-change effects discussed for the design condition, namely the one associated to the incidence and the one associated to the front loading,

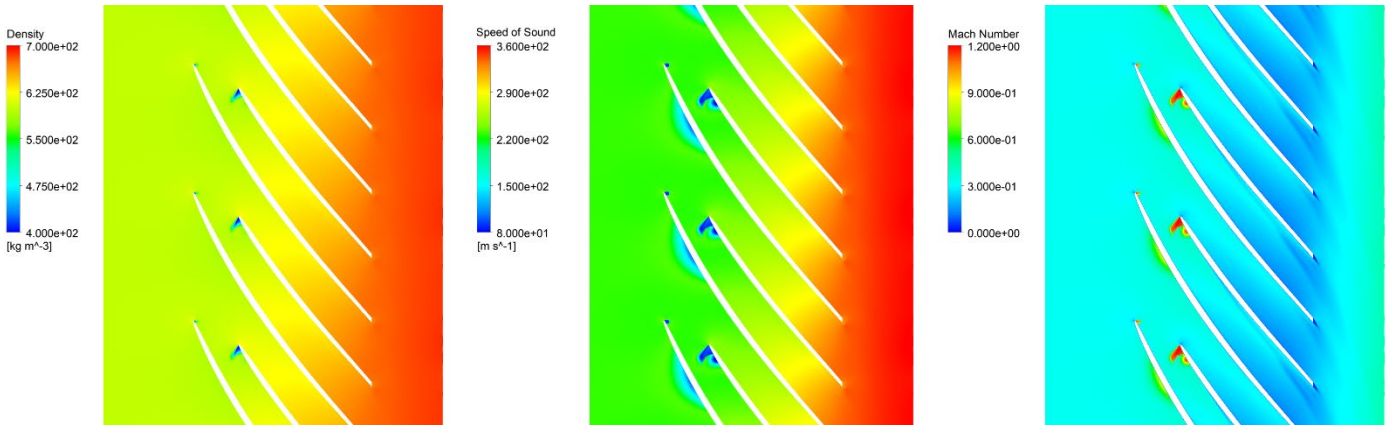

FIGURE 10: DISTRIBUTIONS OF DENSITY (LEFT), SPEED OF SOUND (CENTRE), AND RELATIVE MACH NUMBER (RIGHT) ON THE BLADE-TO-BLADE SURFACE AT 50% SPAN FOR LOW-TEMPERATURE INTAKE CONDITION, 110% FLOW RATE

appear now combined. By increasing the flow rate, the incidence on the main blade becomes negative (about -5°), thus triggering a severe local suction on the pressure side of the leading edge. The subsequent phase change is clearly visible in the density and speed of sound distributions. Moreover, the increase of flow rate enhances the front loading of the main and splitter blades, activating small regions of low speed of sound.

Besides these local effects, a new and broad two-phase feature appears at the leading edge of the splitter blade, induced by a wider suction region between the splitter blade and the adjacent main blade. This effect is caused by the blockage of the splitter blades within the main-blade channel.

The three phenomena discussed above appear on a wider scale in the shroud region, since the higher relative flow velocity with respect to the other sections triggers higher suction. Figure 11 reports the distributions of density, speed of sound and relative Mach number on a blade-to-blade surface placed at 90% span. The negative incidence on the main blade (about -3°) triggers a wide region of

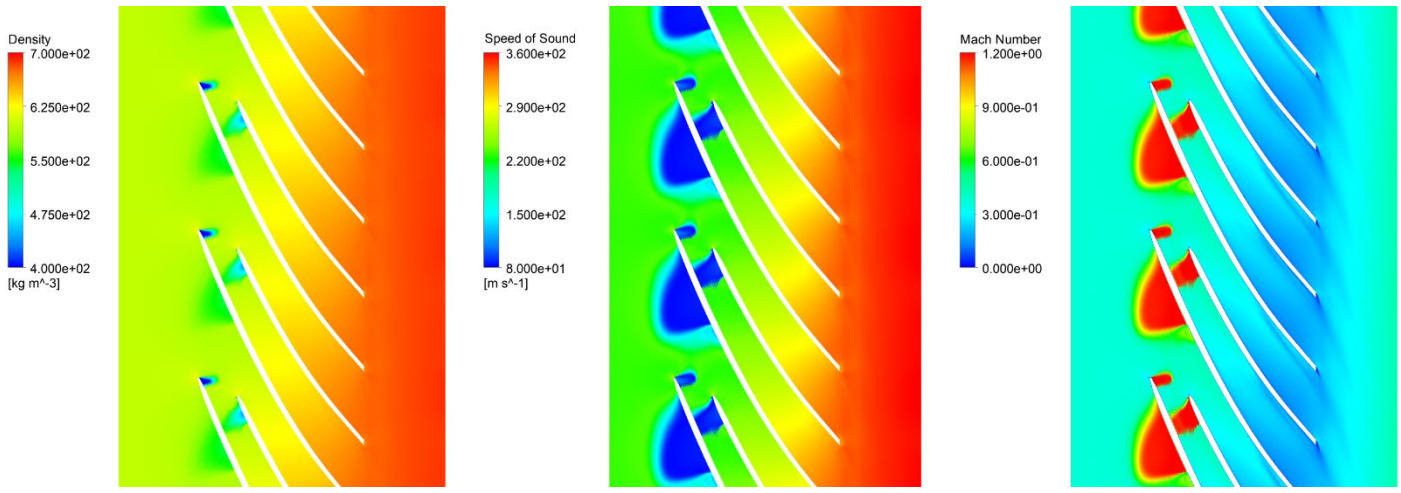

FIGURE 11: DISTRIBUTIONS OF DENSITY (LEFT), SPEED OF SOUND (CENTRE), AND RELATIVE MACH NUMBER (RIGHT) ON THE BLADE-TO-BLADE SURFACE AT 90% SPAN FOR LOW-TEMPERATURE INTAKE CONDITION, 110% FLOW RATE

phase change on the pressure side of the main blade; moreover, the increased front loading induces and extremely wide region of phase change on the suction side of the main blade, where the vapour quality rises to 0.17. This supersonic flow region activates a relatively strong shock, after that the two-phase region terminates. This shock does have an impact on the compressor performance, since it triggers a local boundary layer separation in the front section of the main blade.

A further relevant effect arises within the bladed channel and it is related to the blockage of the splitter blade. At this section, the local expansion leads to vapour qualities of 0.25-0.3 and the two-phase region extends enough to cover entirely one of the channels between the main and the splitter blade, leading there to the onset of a sonic line across the entire channel.

To depict in a three-dimensional fashion the relevance of phase change, Figure 12 reports the isobaric surface corresponding to the saturation pressure for 90%, 100% (design) and 110% flow rate. For low flow rate, which features a general positive incidence, only local suctions at the leading edge of the main and splitter blade appear all along the blade span, while the suction due to front loading takes place only above 80% span. For the design flow rate, the suction at the leading edge reduces (thanks to the optimal incidence all along the span) but the one due to front loading increases, even though appearing only above 80% span. For high flow rate, wide regions of the flow feature excursion in the two-phase region: at the leading edge of the blades all along the span due to negative incidence, in the semi-bladed region due to front loading above midspan, within the channel due to splitter blockage above 80% span.

These results indicate that the chocking limit for this sCO_2 compressor should be expected at much lower flow rate with respect to what can be estimated with a mean-line approach.

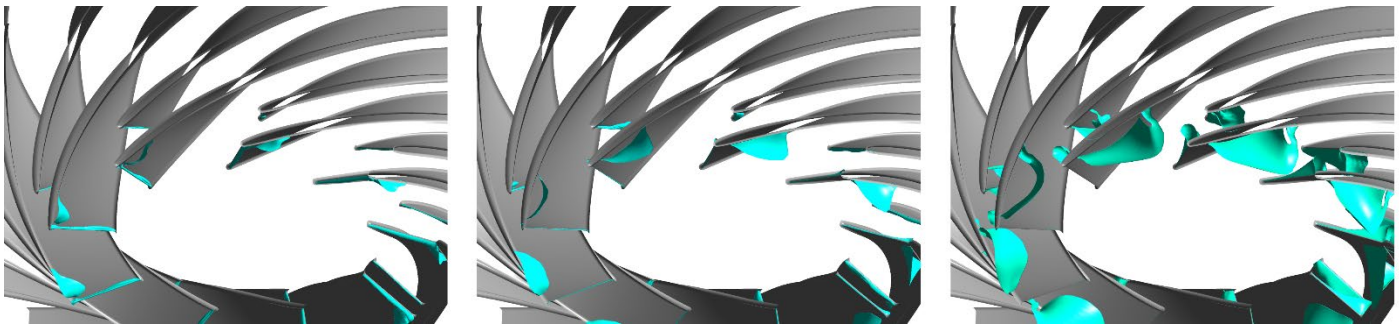

FIGURE 12: SATURATION ISOBARS FOR 90% (LEFT), 100% (CENTER), AND 110% (RIGHT) OF THE DESIGN FLOW RATE

DISCUSSION ON THE THERMODYNAMIC MODEL

In the previous section, flow simulations highlighted a reduction in the compressor range, prompted by an earlier onset of the choking limit. The drop in the speed of sound, crossing the saturation limit, was recognized as the leading cause. The peculiar behavior of the speed of sound in the two-phase domain followed the assumptions of mechanical and thermodynamic equilibrium [18]. This latter assumption produces a discontinuity of the speed of sound across the saturation curve because of a kink in the thermodynamic properties.

As a drawback, the model, also known as homogeneous equilibrium model (HEM), tends to underestimate the speed of sound, especially at low vapor quality (see [29] and references therein).

Many reasons can prevent the establishment of a thermodynamic equilibrium. First, the finite vaporization rate of the liquid may make the phase-change occur at a lower pressure than the saturation one. Moreover, the meta-stable portion is not expected to vanish instantaneously when phase change commences, but its decay will depend on several factors (e.g. the heat-transfer intensity between the meta-stable bulk and the two-phase portion, the expansion rate). To this end, a three-phase model (metastable liquid and saturated liquid and vapor) was proposed [30]. The associated speed of sound, though reducing as the phase change occurs, results higher than that predicted by the HEM; the corresponding quantitative discrepancy depends on the local fraction of meta-stable liquid. Even neglecting meta-stable flows, the heat transfer rarely involves the whole two-phase bulk, but it is more likely limited to those portion of each phase that are close to the interface [31]. Still, a relative velocity between phases may also be present, thus relaxing the assumption of mechanical equilibrium as well.

To sum up, sCO_2 small compressor sizes, combined with the usually high rotational speed to ensure competitive efficiency, suggest that meta-stable and other non-equilibrium phenomena might occur. In this perspective, the indications derived from the present study can be regarded as a safety margin in the operation of the compressor, suggesting caution when the intake conditions of the fluid are close to the critical point. Detailed flow measurements on representative compressor geometries could help to better understand and quantify these phenomena, as well as their subsequent impact on compressor performance.

CONCLUSION

This paper has presented a computational investigation on the aerodynamics of a centrifugal compressor operating in proximity of the CO_2 saturation curve, for that cavitation/flashing is likely to occur in local regions of the compressor intake. The overall operation parameters and the performance of the compressor have been discussed on the basis of a mean-line prediction tool featuring a LUT approach for thermodynamic modeling, which highlights the potential onset of phase change due to the blockage connected to the leading edge of the blades.

The compressor aerodynamics has been investigated in detail by resorting to a non-conventional CFD set-up which features a barotropic-fluid model to take into account the volumetric behavior of the fluid in both the single-phase and the two-phase thermodynamic regions, under the hypothesis of thermal and mechanical equilibrium between the phases. The CFD formulation was verified against compressible flow experiments in a nozzle, where the sCO_2 is operated in thermodynamic conditions close to the ones of interest for the present study, obtaining excellent agreement.

The application of the barotropic CFD model to the compressor has revealed that the phase change might occur in the intake of the compressor according to three main mechanisms: (i) acceleration in the leading edge region due to non-null incidence, (ii) acceleration on the front suction side of the blade due to front loading; (iii) acceleration in the whole channel due to the blockage of the leading edge, especially for the splitter blade. This latter effect, in particular, seems to be the most restrictive in terms of choke margin on the compressor, because of the severe drop of speed of sound across the phase change.

The relevance of the two-phase effects discussed in this paper indicates that an accurate estimate of the speed of sound in multi-phase conditions is crucial for the design and analysis of sCO_2 compressors. Future studies will incorporate non-equilibrium phase change models within the present computational framework, to investigate their quantitative impact on the prediction of sCO_2 compressor aerodynamics and performance. The degree of non-equilibrium featuring the phase change in sCO_2 compressors remains, however, an open question that demands experimental and computational investigations.

ACKNOWLEDGEMENTS

This work was supported by the sCO_2-flex project, funded from the European Union's Horizon 2020 research and innovation programme under grant agreement N° 764690. The authors would like to express their gratitude to Baker Hughes for providing the permission to proceed with publication and to Massimo Camatti for supporting this activity.

REFERENCES

[1] F. Crespi, G. Gavagnin, D. Sanchez and G. S. Martinez, "Supercritical carbon dioxide cycles for power generation: A review," *Applied Energy,* pp. 152-183, 2017.

[2] K. Brun, P. Friedman and R. Dennis, Fundamentals and Applications of Supercritical Carbon Dioxide (sCO2) Based Power Cycles, Woodhead Publishing, 2017.

[3] A. Ameli, A. Afzalifar, T. Turunen-Saaresti and J. Backman, "Effects of real gas model accuracy and operating conditions on supercritical CO2 compressor performance and flow field," *Journal of Engineering for Gas Turbines and Power,* vol. 140, no. 1, p. 062603, 2018.

[4] N. D. Baldadjiev, C. Lettieri and Z. S. Spakovszky, "An investigation of real gas effects in supercritical CO2 centrifugal compressors," *Journal of Turbomachinery,* vol. 137, no. 9, p. 091003, 2015.

[5] T. C. Allison and A. McClung, "Limiting Inlet Conditions for Phase Change Avoidance in Supercritical CO2 Compressors," in *ASME Turbo Expo 2019*, Phoenix, Arizona, USA , 2019.

[6] C. Lettier, D. Paxson, Z. Spakovszky and P. Bryanston-Cross, "Characterization of nonequilibrium condensation of supercritical carbon dioxide in a de laval nozzle," *Journal of Engineering for Gas Turbines and Power,* vol. 140, no. 4, p. 041701, 2017.

[7] J. S. Noall and J. J. Pasch, "Achievable Efficiency and Stability of Supercritical CO2 Compression Systems," in *Supercritical CO2 Power Cycle Symposium*, Pittsburgh, Pennsylvania, 2014.

[8] R. Pecnik, E. Rinaldi and P. Colonna, "Computational fluid dynamics of a radial compressor operating with supercritical CO2," *Journal of Engineering for Gas Turbines and Power,* vol. 134, no. 12, p. 122301, 2012.

[9] A. Ameli, T. Turunen-Saaresti and J. Backman, "Numerical investigation of the flow behavior inside a supercritical CO2 centrifugal compressor," *Journal of Engineering for Gas Turbines and Power ,* vol. 140, no. 6, p. 122604, 2018.

[10] A. Hosangadi, Z. Liu, T. Weathers, V. Ahuja and J. Busby, "Modeling Multiphase Effects in CO2 Compressors at Subcritical Inlet Conditions," *Journal of Engineering for Gas Turbines and Power ,* vol. 141, no. 8, p. 081005, 2019.

[11] K. Brinckman, A. Hosangadi, Z. Liu and T. Weathers, "Numerical Simulation of Non-Equilibrium Condensation in Supercritical CO2 Compressors," in *ASME Turbo Expo 2019*, Phoenix, Arizona, USA , 2019.

[12] S. Wright, R. Radel, M. Vernon, G. Rochau and P. Pickard, "Operation and Analysis of a Supercritical CO2 Brayton Cycle," SANDIA REPORT, SAND2010-0171, Albuquerque, New Mexico, 2010.

[13] R. Span and W. Wagner, "A New Equation of State for Carbon Dioxide Covering the Fluid Region from the Triple-Point Temperature to 1100 K at Pressures up to 800 MPa," *Journal of Physical and Chemical Reference Data,* vol. 25, pp. 1509-1596, 1996.

[14] E. W. Lemmon, H. B. Bell, M. L. Huber and M. O. McLinden, *NIST Standard Reference Database 23: Reference Fluid Thermodynamic and Transport Properties-REFPROP, Version 10.0, National Institute of Standards and Technology,* 2018.

[15] A. Romei, P. Gaetani, A. Giostri and G. Persico, "The role of turbomachinery perfomance in the optimization of supercritical carbon dioxide power systems," *Journal of Turbomachinery,* vol. 142, no. 7, p. 071001, 2020.

[16] F. R. Menter, "Two-Equation Eddy-Viscosity Turbulence Models for Engineering Applications," *AIAA Journal,* vol. 32, no. 8, pp. 1598-1605, 1994.

[17] E. Guidotti, L. Tapinassi, L. Toni, L. Bianchi, P. Gaetani and G. Persico, "Experimental and Numerical Analysis of the Flow Field in the Impeller of a Centrifugal Compressor Stage at Design Point," *ASME Turbo Expo 2011*, Vancouver, BC, Canada , 2011.

[18] N. R. Nannan, A. Guardone and P. Colonna, "On the fundamental derivative of gas dynamics in the vapor–liquid critical region

of single-component typical fluids," *Fluid Phase Equilibria,* vol. 337, pp. 259-273, 2013.

[19] M. Nakagawaa, M. Serrano Beranaa and A. Kishinec, "Supersonic two-phase flow of CO2 through converging–diverging nozzles for the ejector refrigeration cycle," *International Journal of Refrigeration,* vol. 32, pp. 1195-1202, 2009.

[20] K. Banasiak and A. Hafner, "Mathematical modelling of supersonic two-phase R744 flows through converging–diverging nozzles: The effects of phase transition models," *Applied Thermal Engineering,* vol. 51, no. 1, pp. 635 - 643, 2013.

[21] A. Romei and G. Persico, "Computational fluid-dynamic modeling of two-phase compressible flows of carbon dioxide in supercritical conditions," *Submitted to Applied Thermal Engineering.*

[22] P. Gaetani, G. Persico, A. Mora, V. Dossena and C. Osnaghi, "Impeller-vaned diffuser interaction in a centrifugal compressor at off design conditions," *Journal of Turbomachinery,* vol. 134, no. 6, p. 061034, 2012.

[23] M. R. Galvas, "FORTRAN program for predicting off-design performance of centrifugal compressors," NASA TN D-7487, 1973.

[24] W. Jansen, "A method for calculating the flow in a centrifugal compressor impeller when entropy gradients are present," in *Royal Society conference on internal aerodynamics (turbomachinery)*, 1967.

[25] C. Rodgers, " A Diffusion Factor Correlation for Centrifugal Impeller Stalling," *J. Eng. Power,* vol. 100, no. 4, pp. 592-601, 1978.

[26] J. P. D. J. R. C. Johnson, "Losses in vaneless diffusers of centrifugal compressors and pumps. Analysis, experiment, and design.," *Journal of Engineering for Power,* vol. 88, pp. 49-62, 1966.

[27] R. Aungier, Centrifugal Compressors: A Strategy for Aerodynamic Design and Analysis, ASME Press, 1999.

[28] Y. Senoo and Y. Kinoshita, "Influence of inlet flow conditions and geometries of centrifugal vaneless diffusers on critical flow angle for reverse flow," *Journal of Fluids Engineering,* vol. 99, p. 98, 1977.

[29] M. De Lorenzo, P. Lafon, J. M. Seynhaeve and Y. Bartosiewicz, "Benchmark of Delayed Equilibrium Model (DEM) and classic two-phase critical flow models against experimental data," *International Journal of Multiphase Flow,* vol. 92, pp. 112-130, 2017.

[30] C. Lackmè, "Incompleteness of the flashing of a supersaturated liquid and sonic ejection of the produced phases," *International Journal of Multiphase Flow,* vol. 5, pp. 131-141, 1979.

[31] C. E. Brennen, Fundamentals of Multiphase Flows, Cambridge University Press, 2005.